



## Rotating Disk Electrode Voltammetry of Thin Films of Novel Oxide Materials

Ryo H. Wakabayashi,<sup>a</sup> Hanjong Paik,<sup>b</sup> Marc J. Murphy,<sup>b</sup> Darrell G. Schlom,<sup>b</sup> Mario Brützmam,<sup>c</sup> Reinhard Uecker,<sup>c</sup> R. Bruce van Dover,<sup>b</sup> Francis J. DiSalvo,<sup>a</sup> and Héctor D. Abruña<sup>a,\*</sup>

<sup>a</sup>Department of Chemistry, Cornell University, Ithaca, New York 14853, USA

<sup>b</sup>Department of Materials Science and Engineering, Cornell University, Ithaca, New York 14853, USA

<sup>c</sup>Leibniz Institute for Crystal Growth, D-12489 Berlin, Germany

A custom-built apparatus for performing rotating disk electrode voltammetry (RDE) using vapor-deposited, epitaxial, thin film samples as rotating electrodes is described. This method allows for quantitative electrochemical characterization using thin film samples, including those deposited on insulating substrates, and allows for very facile exchange of samples. Cyclic voltammetry and RDE voltammetry of iron ferricyanide in aqueous media were explored to examine if the system causes unusual deviations from ideal hydrodynamic voltammetric behavior. The set-up was also used to examine the ORR activity of a platinum thin film as a model system for a higher-current reaction, relevant to fuel-cell research. Both studies indicated that the set-up did not cause any deviations from anticipated RDE behavior, demonstrating that this is a viable method for performing rotating disk electrode voltammetry of vapor-deposited thin films, with emphasis on those relevant to fuel cell research. The set-up was used to investigate/test the ORR and OER activity of a series of A<sub>2</sub>B<sub>2</sub>O<sub>7</sub> pyrochlore samples.

© 2017 The Electrochemical Society. [DOI: 10.1149/2.1021714jes]

Manuscript submitted July 14, 2017; revised manuscript received November 20, 2017. Published December 23, 2017.

Fuel cells, with a potential for higher energy efficiency, represent a promising alternative technology to internal combustion engines. However, there are many issues that remain to be addressed including the cost of catalysts in order to make the technology more viable and affordable. In today's polymer electrolyte membrane fuel cells (PEMFCs), platinum and/or platinum-based catalysts are used as the catalyst in both the cathode and the anode, which accounts for a significant portion of the cost of fuel cell stacks.<sup>1</sup> A potential alternative in this context is the use of an alkaline electrolyte system. One of the main barriers for the wide-spread deployment of alkaline fuel cells has been the development of high performance anion-exchange membranes,<sup>2</sup> though in recent years, several reports of viable (anionic) hydroxide-conducting membranes,<sup>3-6</sup> that can be used as an alkaline exchange membrane in fuel cell applications, have been reported. This makes the discovery of less expensive alternatives to platinum more important and relevant, especially given that the oxygen reduction reaction (ORR) on platinum still requires at least 300 mV of overpotential to generate the high current densities required in numerous applications; especially automotive. A major potential benefit of an alkaline fuel cell system is that many non-noble metals, and even non-metals,<sup>7-9</sup> are viable candidates as electrocatalysts for the ORR. In particular, oxides are a class of compounds that may be of great interest because many of them are durable (they are already at least partially oxidized) and can be electronically conductive. Manganese and cobalt oxides,<sup>10,11</sup> ruthenium oxide,<sup>12</sup> perovskites<sup>13,14</sup> and some pyrochlore ruthenates<sup>15,16</sup> have been reported as potentially useful ORR catalysts in the past, but in our opinion a systematic study would surely advance the field.

Vapor deposition methods, such as sputtering, are useful tools for depositing thin layers of highly controlled materials useful for numerous applications. In particular, molecular beam epitaxy (MBE) is a deposition method that can produce well defined single crystal surfaces with high structural perfection. These properties make MBE a very useful and attractive technique to fabricate semiconductor devices,<sup>17,18</sup> superconductors,<sup>19</sup> ferromagnets,<sup>20</sup> and other technologically relevant materials. These properties, in principle, are also useful for investigating the electrocatalytic properties of many crystalline compounds, as electrocatalysis is highly sensitive to surface structure and composition.

A main challenge, however, lies in the electrochemical characterization of thin film samples prepared by vapor deposition methods, such as MBE. There have been reports of electrochemical experiments using elaborate custom-made setups,<sup>21</sup> or several simple cyclic

voltammetry experiments using conductive substrates<sup>22-24</sup> or custom-made cells.<sup>25-28</sup> These are complicated systems and generally are not applicable to a significant fraction of thin film samples made using vapor deposition methods, in no small part because many of the most commonly used substrates (silicon, sapphire, etc.) are poor electrical conductors. As such, a facile yet versatile and reproducible way of making a good electrical connection from a deposited sample to the rest of the circuit would be highly beneficial.

In addition, the ORR in particular, is not easy to characterize by cyclic voltammetry, because the concentration profile of oxygen in stagnant solutions is often ill-defined. The ORR also has a two-electron pathway (producing hydrogen peroxide) and a four-electron pathway (producing water), and the two can take place concurrently, further complicating matters. We have previously published a methodology to characterize fuel oxidation reactions on combinatorially sputtered thin films using a scanning-probe differential electrochemical mass spectrometer (DEMS) system that can detect and quantify volatile products,<sup>29</sup> and other research groups have done similar experiments since.<sup>30</sup> However, the products of the ORR, hydrogen peroxide and/or water (deprotonated in alkaline solution), are not detectable using DEMS.

Rotating disk electrode voltammetry (RDE) is a well-established hydrodynamic-transport based voltammetric method that can address these issues by having a well-defined and controlled mass transport. Its use enables the deconvolution of mass transport effects from kinetic effects, a difficult task to do with cyclic voltammetry. By applying the Levich and the Koutecky-Levich equations, parameters such as the number of electrons transferred (electron count), kinetics of electron transfer, and mechanism of electrochemical reactions can be extracted or inferred. There have been a few published RDE voltammetric studies on thin film electrodes,<sup>31-33</sup> but those studies were performed using custom-made substrates that limit the applicable methods of deposition.

Herein, we describe a facile method to turn thin film oxide/substrates into rotating disk electrodes that behave just like a commercial RDE electrode. The setup allows for facile and reproducible assembly and disassembly without damaging the films. We employed sputtered gold and platinum films as model systems to demonstrate that the method is viable.

### Methods/Description of the Instrument

**Instrumentation.**—In order to have a well-characterized electrode as a standard, we used a custom-built magnetron sputtering system at the Cornell Center for Materials Research. We deposited

\*Electrochemical Society Member.

<sup>z</sup>E-mail: hda1@cornell.edu

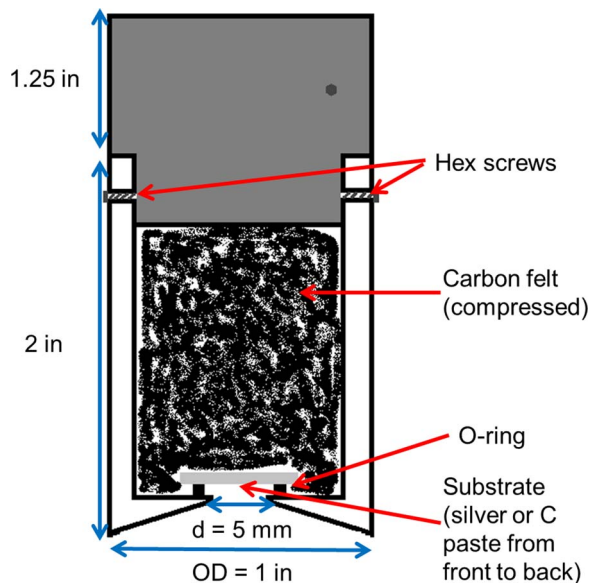


**Figure 1.** Schematic of the custom-made rotating disc electrode system.

approximately 50 nm of gold on top of an approximately 15 nm thick titanium adhesion layer on a microscope glass slide (VWR) that was cut into 10 mm × 10 mm pieces. All films were front-contacted by applying a thin layer of a conductive silver paste (Ted Pella) and/or conductive carbon paint (SPI supplies) from the edge of the film to the back of the substrate.

Figure 1 is a simplified diagram of the electrode system. A 1 inch diameter Teflon rod was machined to fit a 10 mm × 10 mm electrode. In the center, a 5 mm diameter hole was drilled to expose the sample to the solution<sup>d</sup>. A recess was made to place an O-ring (0.25 in), in order to prevent liquid leakage into the sample holder. After placing the back-contacted sample inside, the Teflon holder was packed with carbon felt (Alfa Aesar) and capped with a custom-made, stainless-steel current collector (that could be connected to a Pine rotator) by screwing the stainless steel piece to the Teflon piece using small stainless-steel hex screws. This process was carried using a vice to ensure that the carbon felt was well-packed in order to ensure good electrical conductivity.

A custom-made three-compartment cell (Figure S1) was used for the RDE electrochemical experiments. The main chamber was 2 inches wide, and had an inner glass basket to prevent cavitation (whirlpool). The three compartments were connected at the bottom with medium porosity glass frits, and at the top with simple glass tubing (to equalize the pressure in the three compartments). A graphite rod (Sigma Aldrich) was used as the counter electrode and a homemade saturated silver/silver chloride electrode (Ag/AgCl) was used as the reference electrode. No platinum (or any noble metal) was used in the cell to ensure that there was no contamination from trace Pt from previous experiments<sup>30</sup> (after testing the sputtered Pt and Au films, the cell was soaked in aqua regia for several hours to remove any residual/trace noble metals).

**EIS.**—Electrochemical impedance spectroscopy (EIS) was performed using a Solartron 1280B potentiostat, with either 0.1 M KCl (Macron) or 0.1 M NaOH (Malinkrodt AR) as the electrolyte. A graphite rod was used as the counter electrode, and a home-made saturated Ag/AgCl electrode was used as the reference electrode (when necessary). A 5 mV (peak-to-peak) AC signal was applied, over the frequency range between 1 and 20,000 Hz.

<sup>d</sup>We are using/reporting measurements combining both metric and United States customary system (USCS) units so as to make it easier to reproduce the cell.

**CV and RDE.**—Cyclic voltammetry (CV) and rotating disk electrode voltammetry (RDE) were performed in 0.1 M KCl or 0.1 M NaOH at room temperature. The CV was performed at a scan rate of 20 mV/s (unless otherwise noted), using a Bioanalytical Systems CV-27.  $K_3[Fe(CN)_6]$  (Sigma, ACS reagent) was used as received. The oxygen reduction reaction was studied at room temperature using rotating disk electrode (RDE) voltammetry at a scan rate of 20 mV/s. The solution was saturated with  $O_2$  (Airgas, UHP) by initially bubbling the solution for 15 minutes and 7 minutes after measurements at each rotation rate, in order to keep the solution saturated with oxygen for each recorded scan. During the measurement, the bubbling was stopped to prevent noise in the current induced by bubbles.

Some CV data were averaged using the Savitzky-Golay method (9 points) to remove periodic noise.

**Deposition method of Au.**—An Au thin film was deposited using the CCMR sputtering chamber discussed in above.

**MBE deposition method.**—Complex oxide films were grown using a Veeco GEN 10 dual-oxide MBE chamber. Briefly, commercially available (111) yttrium-stabilized zirconia (YSZ) was used as the substrate for all but one sample. A non-commercial  $Sm_2Ti_2O_7$  (111) substrate was used as the substrate for one sample to achieve isostructural growth (pyrochlore-on-pyrochlore epitaxy).<sup>34</sup> Prior to growth, the YSZ substrates were heated at 1300°C for 3 h in air to obtain an atomically flat surface. The  $Sm_2Ti_2O_7$  (111) substrate was chemomechanically polished by a commercial vendor (CrysTec GmbH) to obtain an atomically flat surface. For the metals on the A-site of the pyrochlore  $A_2B_2O_7-x$  (A = main group metal; Bi or Pb in this work), an over-pressure supply flux ( $1.0 \times 10^{14}$  atoms/cm<sup>2</sup> × sec) was used during growth, which was approximately 10 to 15 times greater than the flux for the B-site metal (transition metal; Ru or Ir in this work) ( $0.3 \times 10^{13}$  atoms/cm<sup>2</sup> × sec). All components were co-supplied simultaneously during the growth. Distilled ozone ( $1.0 \times 10^{-6}$  Torr) was used as the oxidant. The growth temperature was maintained at 500–600°C and monitored with an optical pyrometer.

To determine the optimal single-growth window, where the excess Bi or Pb desorbs (adsorption-controlled growth conditions), in-situ reflection high-energy electron diffraction (RHEED) was used. Thin film crystalline quality was checked by four-circle X-ray diffraction with a two bounce Ge (220) monochromator (Rigaku, Smartlab), and high-resolution rocking curves were measured by adding a two bounce Ge (220) crystal analyzer on the receiving side (triple axis geometry). Film thickness (i.e. growth rate) was limited by the Sn-flux supply, which was consistent with the QCM measurement within ±10% error. The spacing of the XRD thickness fringes (Kiessig fringes) of the main 222 Bragg peak confirmed the film thickness. Rutherford backscattering spectroscopy (RBS) confirmed the film stoichiometry to within ±3%. Cross-sectional high-angle annular dark field (HAADF) scanning transmission electron microscopy (STEM) (FEI Technai F-20 TEM/STEM in STEM mode with a beam voltage of 200 keV) revealed the interface structure. The surface morphology was characterized by atomic force microscopy (AFM). For XRD, RBS, STEM, and AFM data, refer to future published literature by Paik and Schlom.

## Operations/Results and Discussion

**EIS.**—Our setup has a somewhat unconventional method for making electrical connection from the electrode to the current collector. To investigate the validity of this method, reduction (and oxidation) of  $K_3[Fe(CN)_6]$  (0.81 mM) in 0.1 M KCl, a well-studied electrochemical reaction, was investigated on a sputtered gold film (approx. 50 nm thick) electrode, and the results were compared to those of a bulk Au electrode (dia = 5 mm).

Figure 2 shows the Nyquist plots of the Au thin film and bulk Au electrodes in 0.1 M KCl (with no redox-active species in solution). The total linear resistance (first x-intercept, i.e. impedance at which there is no capacitive contribution) was approximately 190 ohms for the thin film, whereas it is approximately 90 ohms for the bulk gold electrode.

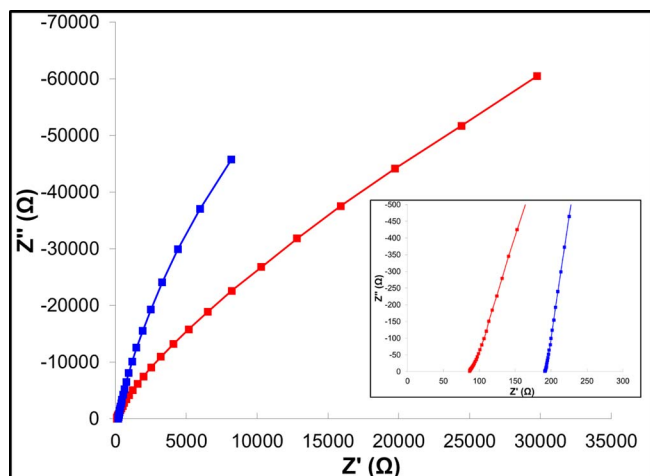


**Figure 2.** Nyquist plots of Au film (blue) and bulk Au (red) in 0.1 M KCl, at OCP, 5 mV AC, 20,000 Hz – 1 Hz ( $Z'$  and  $Z''$  increase as the frequency decreases).

EIS was performed with the reference electrode being placed directly adjacent to the working electrode in order to determine if the rather long distance between the compartment introduced an additional resistance (ohmic drop), but it did not (see Figure 3). It is clear that the distance between the reference and the working electrode in this set-up did not introduce a significant/additional ohmic drop.

**CV and RDE of  $K_3[Fe(CN)_6]$ .**—The cyclic voltammetric profiles in 0.1 M KCl did not show an evidence of significant  $iR$ -drops (Figure 4a). In fact, the surface gold oxidation and reduction peaks were more visible on the CV profile of the Au thin film electrode (Figure 4b). Noisy regions of the CV of the thin Au film around 0 V vs. Ag/AgCl in the negative-going sweep (Figure 4b) could be due to the local pH change induced by the surface oxide reduction, since the electrolyte was not buffered. This, however, is not a major concern for the remaining experiments, as the potential range used for the study of  $K_3[Fe(CN)_6]$  did not include this region (Red CV profiles in Figure 4). The difference in series resistance, however, was somewhat noticeable in the cyclic voltammograms (CV) of  $K_3[Fe(CN)_6]$  in 0.1 M KCl (Figure 5) on sputtered gold films, performed at various scan rates. The peak-to-peak separation between the oxidation and the reduction

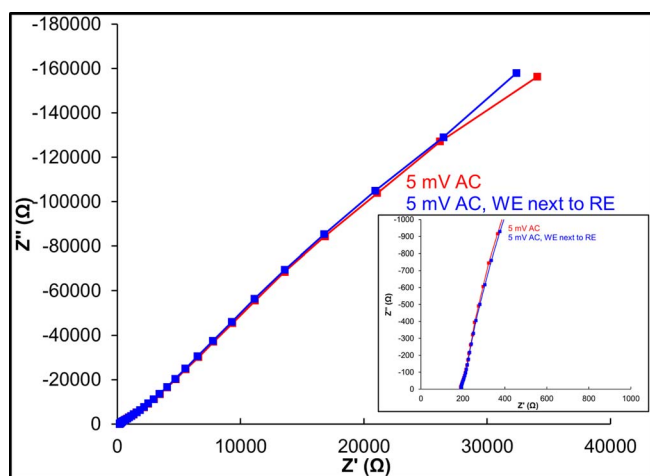


**Figure 3.** Nyquist plots of Au film with RE in its own compartment (red) and with the reference electrode moved directly adjacent to the working electrode (blue) in 0.1 M KCl, at OCP, 5 mV AC, 20,000 Hz – 1 Hz ( $Z'$  and  $Z''$  increase as the frequency decreases).

of ferricyanide increased with increasing scan rate when the thin film Au was used as the electrode, indicating some resistance issues. On the other hand, there is only a minimal increase in the peak-to-peak separation as a function of the scan rate on the CV of the same reaction using the bulk gold electrode. Still, carrying out experiments at relatively slow scan rates (as would be the case for RDE voltammetry) would eliminate any concerns.

An ideal rotating disk electrode has a flat surface with an axis rotation, so as to establish laminar flow. As evident in Figure 1, the holder described in this paper has two geometric irregularities; the electrode is recessed by the thickness of the O-ring (approx. 2 mm), and the Teflon surface slants downward toward the electrode. To investigate the effect of such irregularities, the reduction of  $K_3[Fe(CN)_6]$  (0.81 mM) in 0.1 M KCl was investigated using the standard/conventional RDE technique at a scan rate of 20 mV/s. Figure 6 shows the results of the experiment. The kinetic regions (including the onset potential) of the two RDE voltammograms look nearly identical, aside from the systematic offset in current introduced by the slight difference in the double layer current. Applying the Levich equation  $i_L = 0.620 n F A D^{2/3} \omega^{1/2} \nu^{-1/6} C_0$  ( $F$  = Faraday constant,  $A$  = area of the electrode,  $n$  = number of electrons transferred, and  $\nu$  = kinematic viscosity  $9.913 \times 10^{-3} \text{ cm}^2/\text{s}$  for 0.1 M KCl<sup>35</sup>) at 0.06 V vs. Ag/AgCl (Figure 6d), the diffusion coefficient ( $D$ ) was determined to be  $7.6 \times 10^{-6} \pm 0.7 \text{ cm}^2/\text{s}$ , which is very close to the reported value in the literature ( $7.6 \times 10^{-6} \text{ cm}^2/\text{s}$ <sup>36</sup>). As a comparison, the identical experiment was performed in the same solution using a bulk Au electrode (Figure 6a). Using the same assumptions, the diffusion coefficient was determined to be  $7.5 \times 10^{-6} \text{ cm}^2/\text{s}$ . It should be noted that for the Levich plot of thin film RDE, the intercept of the best-fit line is below zero, when in theory, it should be zero (or often times positive). While it is difficult to unambiguously ascribe the cause for such a phenomenon, the slope is still linear with a very high coefficient of determination ( $r^2$ ), which is sufficient for extracting parameters like the diffusion coefficient and the number of electrons transferred. Therefore, we do not believe this to be a significant problem.

**ORR on Pt thin film.**—One of the greatest benefits of RDE voltammetry is the ability to quantify electrochemical redox processes. RDE voltammetry of the ORR was carried out in 0.1 M NaOH using a sputtered Pt electrode (see Figure 7a). The voltammetric profiles are in line with reported ORR voltammograms of bulk Pt. The Levich plot (Figure 7b), derived from current densities at -0.6 V vs. Ag/AgCl yielded an excellent best-fit line ( $r^2 = 0.9999$ ) and  $n = 3.97$  electrons from the Levich equation (assuming a diffusion coefficient of  $O_2$  in water of  $D = 1.93 \times 10^{-5} \text{ cm}^2/\text{s}$ ,  $C_0 = 1.26 \times 10^{-3} \text{ M } O_2$  at saturation, and kinematic viscosity  $\nu = 1.07 \times 10^{-2} \text{ cm}^2/\text{s}$ , all based on values reported in the literature<sup>37</sup>). Though the mass-transport limited region of Figure 7a is not strictly flat, it shows negligible to no difference on the Levich plot (Figure 7b). General current and voltammetric profiles are in line with reported values as well.<sup>38–43</sup> This is further confirmation that the dimensions and configurations of the holder/electrode are sufficiently optimized for testing thin-film electrodes in electrochemical cells for reactions such as the ORR.

**ORR and OER on MBE samples.**—To demonstrate the use of this apparatus on samples of interest for research science, we investigated a series of samples deposited by MBE.

Figure 8 shows the Nyquist plots of oxide thin film electrodes ( $Pb_2Ir_2O_7$  and  $IrO_2$ )(MBE) in 0.1 M NaOH. It is clear that the oxide thin films are more resistive than a conventional electrode, with the series resistance (approximated from the first X-intercept) being about twice that of the GC (glassy carbon) electrode in the case of  $IrO_2$ , and two orders of magnitude higher in the case of  $Pb_2Ir_2O_7$ .

Figure 9a presents a metacomparison of RDE voltammograms of various pyrochlore oxides, grown using the Veeco GEN 10 dual-oxide MBE chamber, in  $O_2$ -saturated 0.1 M NaOH at 1600 rpm. The shallow slopes of the voltammograms strongly suggest that there

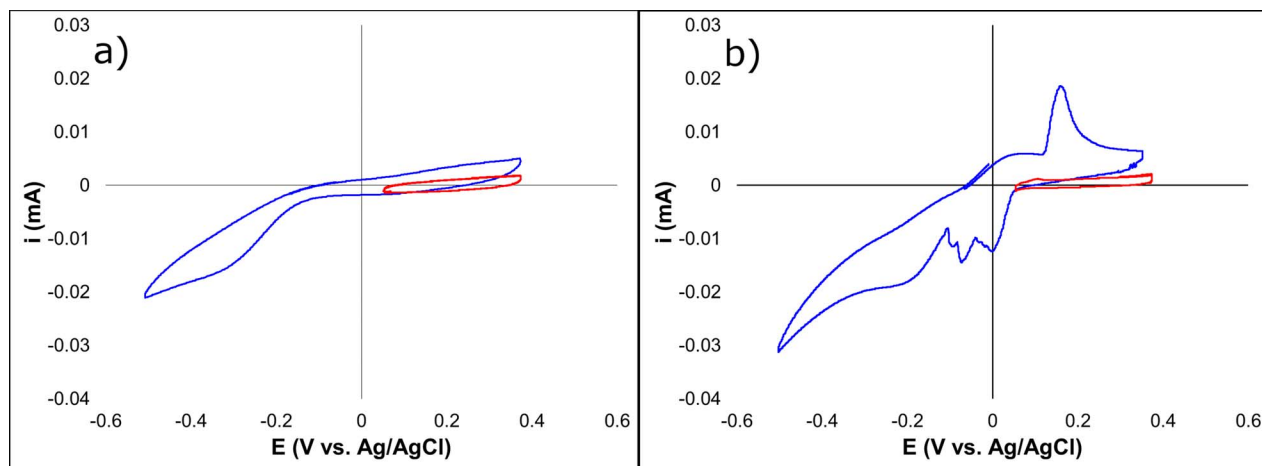


**Figure 4.** Cyclic voltammograms of bulk (a) and film (b) Au in 0.1 M KCl. Scan rate 20 mV/s. Red: potential range used for CV of  $K_3[Fe(CN)_6]$ .

is a significant  $iR$  drop in these samples; therefore, the most useful parameter to compare is the onset potential.

We tested a series of  $A_2B_2O_7$  pyrochlore samples. The following discussion centers on  $Bi_2Ru_2O_7$  (111) as the standard and will serve as the basis to discuss the effects of substitution and other changes. Among the  $Bi_2Ru_2O_7$  samples (Figure 9a), there is little to no dependence of the response on thickness (20 nm vs. 10 nm) or crystallographic orientation (111 vs. 001). Similarly, introducing 0.6% biaxial compressive strain<sup>44</sup> by epitaxial growth on  $Sm_2Ti_2O_7$  also

appeared to have little (if any) effect on the electrocatalytic activity. The onset potentials (defined as  $E$  when  $j = 0.1 \text{ mA/cm}^2$ ) are all approximately  $-0.2 \text{ V}$  vs. Ag/AgCl. The sample with the best onset potential of the series (20 nm) was  $-0.20 \text{ V}$  and the worst (001) was  $-0.23 \text{ V}$ . Substitution on the B sites of the pyrochlore structure with iridium and forming  $Bi_2(Ru/Ir)_2O_7$  samples (shades of blue in Figure 9c) increased the  $iR$  drop significantly, even with a small amount of Ir. However, the onset potential remained virtually unchanged. Substitution on the A site with Pb to form  $Pb_2Ru_2O_7$ , however, improved

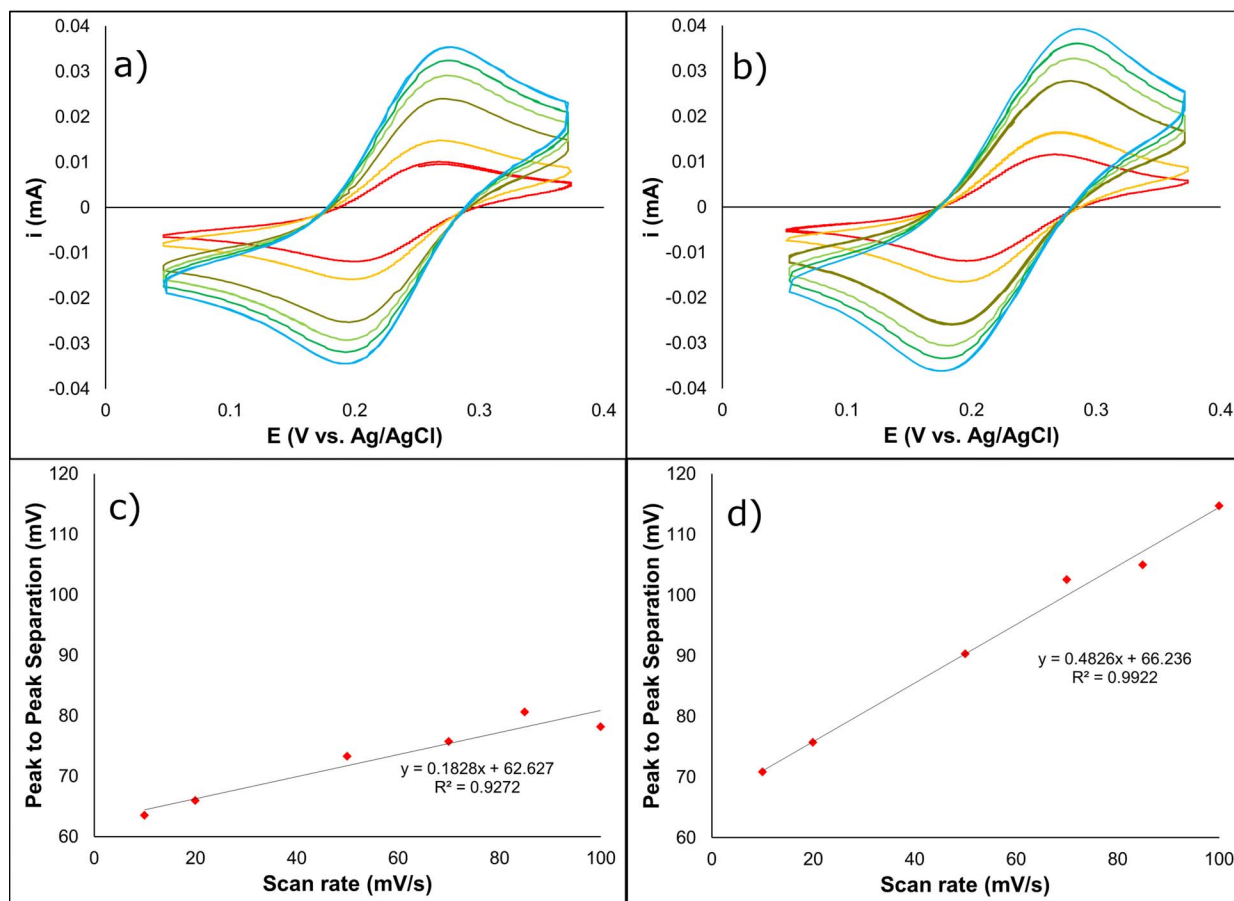


**Figure 5.** Cyclic voltammogram of 0.81 mM  $K_3[Fe(CN)_6]$  in 0.1 M KCl on bulk (a) Au and sputtered gold film (b) (approx. 50 nm thick), and peak-to-peak separations of the oxidation and reduction peaks (c is for bulk Au, d is for thin Au film). Scan rates are 10 (red), 20 (orange), 50 (mustard), 70 (light green), 85 (green) and 100 (light blue) mV/s.

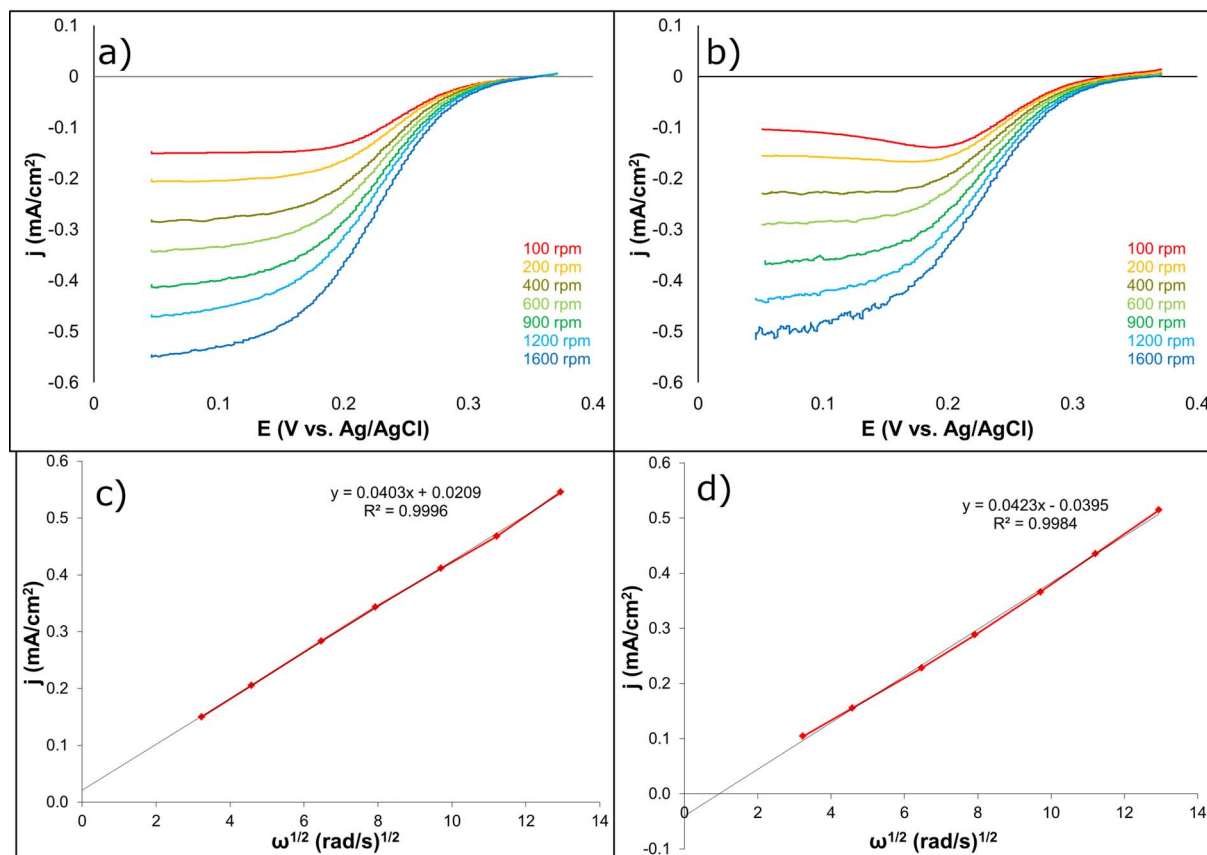
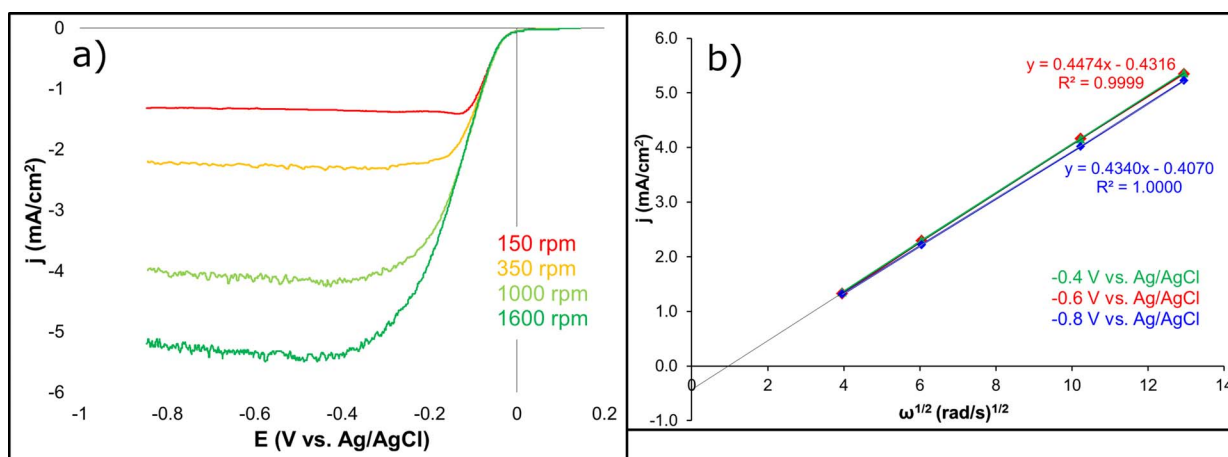


**Figure 6.** Rotating disk electrode voltammetry of  $0.81 \text{ mM K}_3[\text{Fe}(\text{CN})_6]$  in  $0.1 \text{ M KCl}$  on bulk Au (a) and Au film (b). (c) Levich plots at  $0.06 \text{ V vs. Ag/AgCl}$  of bulk Au and Au film (d).

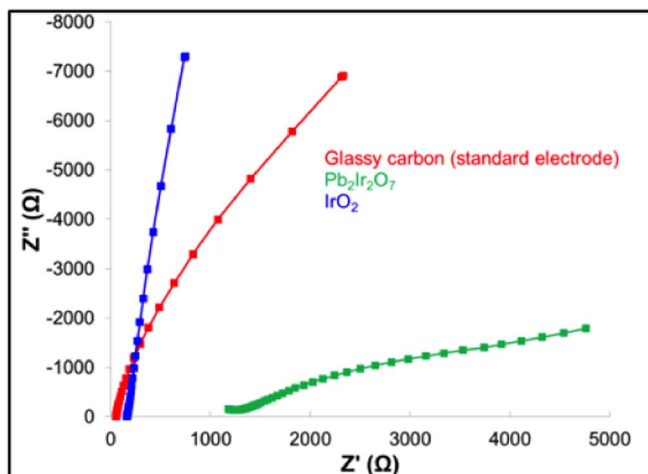
the onset potential considerably, to  $-0.14 \text{ V vs. Ag/AgCl}$  (Figure 9b). Finally, substitution of both the A site and B site from  $\text{Bi}_2\text{Ru}_2\text{O}_7$  to  $\text{Pb}_2\text{Ir}_2\text{O}_7$  significantly decreased the electrocatalytic activity (and, likely, conductivity), with the onset potential decreasing to  $-0.30 \text{ V vs. Ag/AgCl}$  (green). Perhaps these results are not surprising, as  $\text{IrO}_2$  (mustard) is a very poor ORR catalyst (pink line). In short, Pb appears to be a more favorable candidate than Bi for the A site cation, and Ru is a far superior B site cation when compared to Ir.

Figure 10 shows linear sweep voltammograms of selected samples, deposited by MBE, examining the OER in  $\text{O}_2$ -saturated  $0.1 \text{ M}$

$\text{NaOH}$ . The  $\text{Bi}_2\text{Ru}_2\text{O}_7$  sample shows an onset potential of  $+0.58 \text{ V vs. Ag/AgCl}$ . Substitution of the B site with Ir ( $\text{Bi}_2\text{Ir}_2\text{O}_7$ ) does not significantly alter the electrocatalytic activity for the OER. Interestingly, two samples of  $\text{Bi}_2\text{Ir}_2\text{O}_7$  showed dramatically different activities (blue vs. dotted blue), likely dependent on deposition parameters. Partial substitution of Ir with Ru, forming  $\text{Bi}_2(\text{Ir/Ru})_2\text{O}_7$  (shades of blue) improved the onset potential and the kinetics slightly, in sharp contrast to the previous figure. Since bulk  $\text{IrO}_2$  is one of the best OER catalysts known,<sup>45</sup> this result is consistent with those observations.  $\text{IrO}_2$  (mustard), however, showed very poor activity, perhaps



**Figure 7.** (a) RDE voltammogram of a sputtered Pt thin film electrode in oxygen-saturated  $0.1 \text{ M NaOH}$ , measured using a home-made electrode setup. (b) Levich plot, generated from current densities at  $-0.4 \text{ V}$  (green),  $-0.6 \text{ V}$  (red) and  $-0.8 \text{ V}$  (blue) vs. Ag/AgCl, with equations for the linear regression lines for the data from  $-0.6 \text{ V}$  and  $-0.8 \text{ V}$ .



**Figure 8.** Nyquist plots of selected MBE oxide samples ( $\text{Pb}_2\text{Ir}_2\text{O}_7$  pyrochlore and  $\text{IrO}_2$ ). A glassy carbon electrode represents a standard electrode. Data acquired by the open circuit potential (OCP), 10 mV AC, 20,000 Hz – 1 Hz ( $Z'$  and  $Z''$  increase as the frequency decreases).

because of the poor conductivity of the thin film sample, as shown in Figure 8. Substitution of Bi with Pb ( $\text{Pb}_2\text{Ru}_2\text{O}_7$ ) did not alter the electrocatalytic activity. In fact, the second sample (dotted line of the same lime green) has one of the best onset potentials ( $\sim 0.55$  V vs. Ag/AgCl).  $\text{Pb}_2\text{Ir}_2\text{O}_7$  (green). Substitution of both the A and B sites of

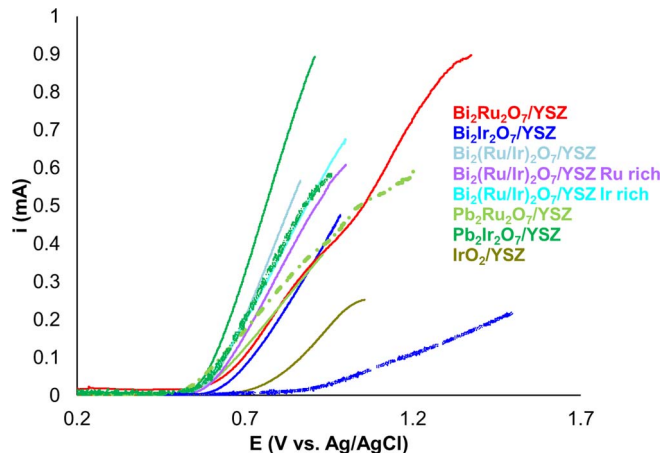


**Figure 10.** RDE metacomparison of the oxygen evolution reaction (OER) in oxygen-saturated 0.1 M NaOH using MBE-grown pyrochlore thin film electrodes. Dotted lines indicate different samples of the same nominal composition. All samples are (111), unless otherwise indicated.

$\text{Bi}_2\text{Ru}_2\text{O}_7$ , improved the electrocatalytic activity considerably (onset potential  $\sim 0.55$  V vs. Ag/AgCl, steeper slope). However, it should be noted that a significant difference was observed between samples (two different lime green lines).

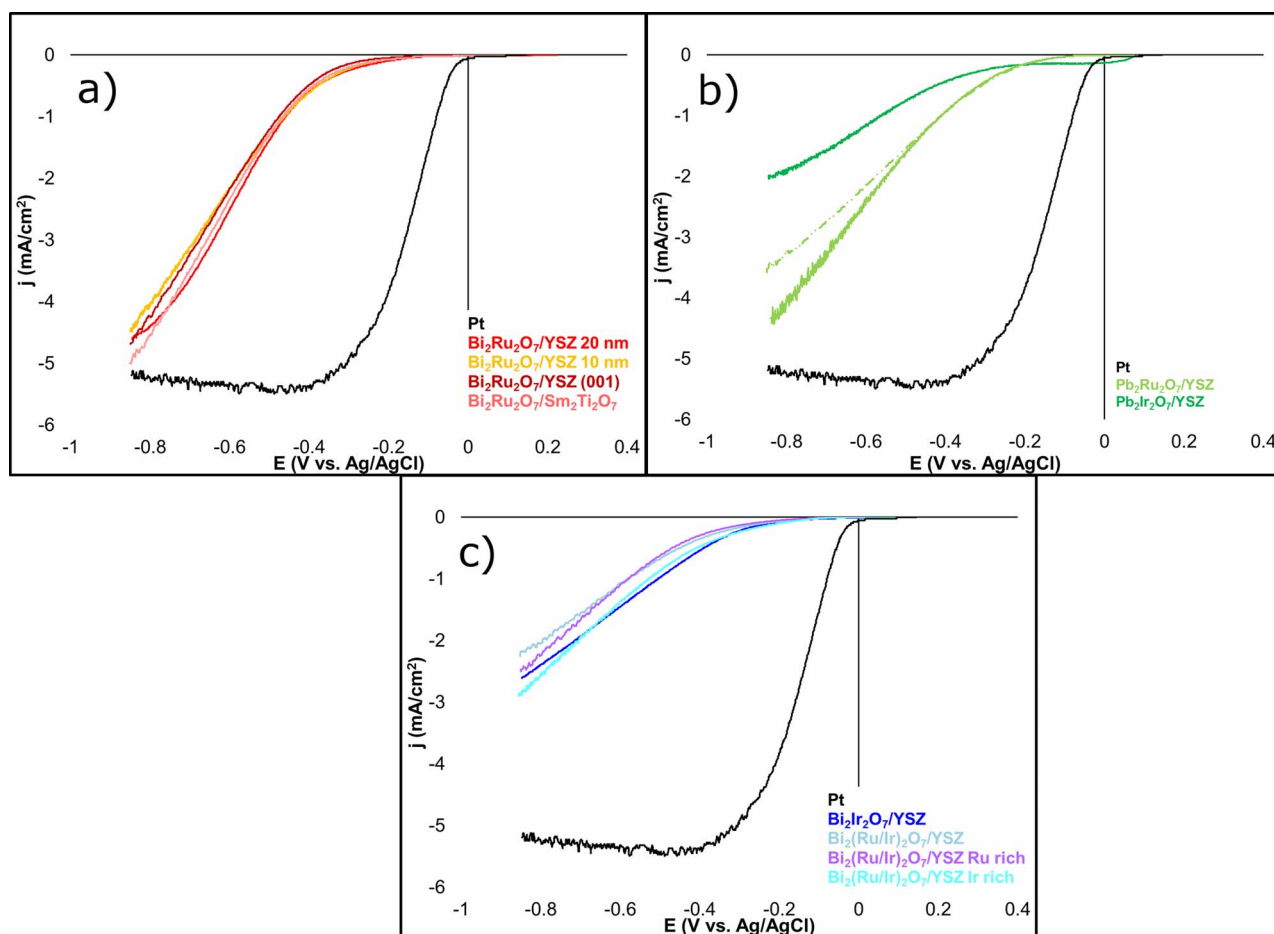


**Figure 9.** RDE metacomparison of the oxygen reduction reaction (ORR) in oxygen-saturated 0.1 M NaOH using MBE-grown pyrochlore thin film electrodes: (a)  $\text{Bi}_2\text{Ru}_2\text{O}_7$ , (b)  $\text{Pb}_2\text{X}_2\text{O}_7$ , and (c)  $\text{Bi}_2(\text{Ru}/\text{Ir})_2\text{O}_7$ . The voltammetric profile for Pt is reproduced/copied from Figure 7.

## Conclusions

A facile method to perform rotating disk electrode voltammetry on thin film electrodes has been developed. Using sputter-deposited Au and Pt, it was demonstrated to be a robust method that can be used and configured for thin films. This method allows for a more detailed characterization of reactions such as the oxygen reduction reaction and oxygen evolution reaction than simple cyclic voltammetry, using deposited thin film electrodes.

We also studied a series of pyrochlore-structure samples grown by MBE as examples. While many pyrochlores, made via MBE, showed promising electrocatalytic activities in terms of onset potentials, they exhibited significant iR drops. Perhaps as a result, the effects of strain caused by epitaxial growth, or different crystallographic orientation, seem to exhibit negligible differences in the electrocatalytic activity toward the ORR and OER.  $\text{Pb}_2\text{Ru}_2\text{O}_7$  is the most promising candidate for further study.

## Acknowledgments

This work is based upon work supported as part of the Energy Materials Center at Cornell (EMC<sup>2</sup>), an Energy Frontier Research Center funded by the U. S. Department of Energy, Office of Science, and Office of Basic Energy Sciences under Award Number DE-SC0001086. This work was also supported by Cornell University from September 2014 through June 2016. This work made use of the Cornell Center for Materials Research Shared Facilities which are supported through the NSF MRSEC program (DMR-1120296).

## References

- J. Marcinkoski, J. S. Spendlow, A. Wilson, and D. C. Papageorgopoulos, DOE Fuel Cell Technologies Office Record 15015: Fuel Cell System Cost - 2015 [https://www.hydrogen.energy.gov/pdfs/15015\\_fuel\\_cell\\_system\\_cost\\_2015.pdf](https://www.hydrogen.energy.gov/pdfs/15015_fuel_cell_system_cost_2015.pdf) (accessed Apr 17, 2016).
- J. K. Dombrowski and A. E. C. Palmqvist, Recent Progress in Synthesis, Characterization and Evaluation of Non-Precious Metal Catalysts for the Oxygen Reduction Reaction, *Fuel Cells*, **16**, 4 (2016).
- K. J. T. Noonan, K. M. Hugar, H. A. Kostalik, E. B. Lobkovsky, H. D. Abruña, and G. W. Coates, Phosphonium-Functionalized Polyethylene: A New Class of Base-Stable Alkaline Anion Exchange Membranes, *J. Am. Chem. Soc.*, **134**, 18161 (2012).
- H. A. Kostalik, T. J. Clark, N. J. Robertson, P. F. Mutolo, J. M. Longo, H. D. Abruña, and G. W. Coates, Solvent Processable Tetraalkylammonium-Functionalized Polyethylene for Use as an Alkaline Anion Exchange Membrane, *Macromolecules*, **43**, 7147 (2010).
- G. Couture, A. Alaeddine, F. Boschet, and B. Ameduri, Polymeric materials as anion-exchange membranes for alkaline fuel cells, *Prog. Polym. Sci.*, **36**, 1521 (2011).
- S. Gu, R. Cai, T. Luo, Z. Chen, M. Sun, Y. Liu, G. He, and Y. Yan, A Soluble and Highly Conductive Ionomer for High-Performance Hydroxide Exchange Membrane Fuel Cells, *Angew. Chem. Int. Ed.*, **48**, 6499 (2009).
- N. Ramaswamy and S. Mukerjee, Influence of Inner- and Outer-Sphere Electron Transfer Mechanisms during Electrocatalysis of Oxygen Reduction in Alkaline Media, *J. Phys. Chem. C*, **115**, 18015 (2011).
- B. Wang, Recent development of non-platinum catalysts for oxygen reduction reaction, *J. Power Sources*, **152**, 1 (2005).
- X. Ge, A. Sumboja, D. Wu, T. An, B. Li, F. W. T. Goh, T. S. A. Hor, Y. Zong, and Z. Liu, Oxygen Reduction in Alkaline Media: From Mechanisms to Recent Advances of Catalysts, *ACS Catal.*, **5**, 4643 (2015).
- A. C. Queiroz and F. H. B. Lima, Electrocatalytic activity and stability of Co and Mn-based oxides for the oxygen reduction reaction in alkaline electrolyte, *J. Electroanal. Chem.*, **707**, 142 (2013).
- J. Du, C. Chen, F. Cheng, and J. Chen, Rapid Synthesis and Efficient Electrocatalytic Oxygen Reduction/Evolution Reaction of  $\text{CoMn}_2\text{O}_4$  Nanodots Supported on Graphene, *Inorg. Chem.*, **54**, 5467 (2015).
- D. F. Abbott, S. Mukerjee, V. Petrykin, Z. Bastil, N. B. Halck, J. Rossmeisl, and P. Krtil, Oxygen reduction on nanocrystalline ruthenium – local structure effects, *RSC Adv.*, **5**, 1235 (2014).
- T. Poux, A. Bonnefont, G. Kéranguéven, G. A. Tsirlina, and E. R. Savinova, Electrocatalytic Oxygen Reduction Reaction on Perovskite Oxides: Series versus Direct Pathway, *ChemPhysChem*, **15**, 2108 (2014).
- J. Suntivich, H. A. Gasteiger, N. Yabuuchi, H. Nakanishi, J. B. Goodenough, and Y. Shao-Horn, Design principles for oxygen-reduction activity on perovskite oxide catalysts for fuel cells and metal-air batteries, *Nat. Chem.*, **3**, 546 (2011).
- H. S. Horowitz, J. M. Longo, and H. H. Horowitz, Oxygen Electrocatalysis on Some Oxide Pyrochlores, *J. Electrochem. Soc.*, **130**, 1851 (1983).
- R. G. Egddell, J. B. Goodenough, A. Hamnett, and C. C. Naish, Electrochemistry of ruthenates. Part 1.—Oxygen reduction on pyrochlore ruthenates, *J. Chem. Soc. Faraday Trans. 1 Phys. Chem. Condens. Phases*, **79**, 893 (1983).
- C. R. Abernathy, Compound semiconductor growth by metalloorganic molecular beam epitaxy (MOMBE), *Mater. Sci. Eng. R Rep.*, **14**, 203 (1995).
- Ü. Özgür, Y. I. Alivov, C. Liu, A. Teke, M. A. Reshchikov, S. Doğan, V. Avrutin, S.-J. Cho, and H. Morkoç, A comprehensive review of ZnO materials and devices, *J. Appl. Phys.*, **98**, 041301 (2005).
- W. Li-Li, M. Xu-Cun, C. Xi, and X. Qi-Kun, Molecular beam epitaxy and superconductivity of stoichiometric FeSe and  $\text{KxFe}_2\text{-ySe}_2$  crystalline films, *Chin. Phys. B*, **22**, 086801 (2013).
- J. M. D. Coey, M. Venkatesan, and C. B. Fitzgerald, Donor impurity band exchange in dilute ferromagnetic oxides, *Nat. Mater.*, **4**, 173 (2005).
- I. Milošev, H.-H. Strehlow, and B. Navinšek, Comparison of TiN, ZrN and CrN hard nitride coatings: Electrochemical and thermal oxidation, *Thin Solid Films*, **303**, 246 (1997).
- E. L. Miller and R. E. Rocheleau, Electrochemical Behavior of Reactively Sputtered Iron Doped Nickel Oxide, *J. Electrochem. Soc.*, **144**, 3072 (1997).
- E. L. Miller and R. E. Rocheleau, Electrochemical and Electrochromic Behavior of Reactively Sputtered Nickel Oxide, *J. Electrochem. Soc.*, **144**, 1995 (1997).
- A. Z. Ait-Djafer, N. Saoula, H. Aknouche, B. Guedouar, and N. Madaoui, Deposition and characterization of titanium aluminum nitride coatings prepared by RF magnetron sputtering, *Appl. Surf. Sci.*, **350**, 6 (2015).
- M. D. Fleischauer, T. D. Hatchard, G. P. Rockwell, J. M. Topple, S. Trussler, S. K. Jericho, M. H. Jericho, and J. R. Dahn, Design and Testing of a 64-Channel Combinatorial Electrochemical Cell, *J. Electrochem. Soc.*, **150**, A1465 (2003).
- T. D. Hatchard, J. M. Topple, M. D. Fleischauer, and J. R. Dahn, Electrochemical Performance of  $\text{SiAlSn}$  Films Prepared by Combinatorial Sputtering, *Electrochem. Solid-State Lett.*, **6**, A129 (2003).
- S. Guerin, B. E. Hayden, C. E. Lee, C. Mormiche, J. R. Owen, A. E. Russell, B. Theobald, and D. Thompsett, Combinatorial Electrochemical Screening of Fuel Cell Electrocatalysts, *J. Comb. Chem.*, **6**, 149 (2004).
- A. S. Bandarenka, E. Ventosa, A. Maljusch, J. Masa, and W. Schuhmann, Techniques and methodologies in modern electrocatalysis: evaluation of activity, selectivity and stability of catalytic materials, *Analyst*, **139**, 1274 (2014).
- E. D. Rus, H. Wang, A. E. Legard, N. L. Ritzert, R. B. V. Dover, and H. D. Abruña, An exchangeable-tip scanning probe instrument for the analysis of combinatorial libraries of electrocatalysts, *Rev. Sci. Instrum.*, **84**, 024101 (2013).
- S. Cherevko, G. P. Keeley, S. Geiger, A. R. Zeradjanin, N. Hodnik, N. Kulyk, and K. J. J. Mayrhofer, Dissolution of Platinum in the Operational Range of Fuel Cells, *ChemElectroChem*, **2**, 1471 (2015).
- D. F. van der Vliet, C. Wang, D. Tripkovic, D. Strmcnik, X. F. Zhang, M. K. Debe, R. T. Atanasoski, N. M. Markovic, and V. R. Stamenkovic, Mesostructured thin films as electrocatalysts with tunable composition and surface morphology, *Nat. Mater.*, **11**, 1051 (2012).
- C. Z. Deng and M. J. Dignam, Sputtered Cobalt Carbon Nitrogen Thin Films as Oxygen Reduction Electrocatalysts I. Physical and Electrochemical Characterization, *J. Electrochem. Soc.*, **145**, 3507 (1998).
- O. Savadogo, K. Lee, K. Oishi, S. Mitsushima, N. Kamiya, and K.-I. Ota, New palladium alloys catalyst for the oxygen reduction reaction in an acid medium, *Electrochem. Commun.*, **6**, 105 (2004).
- D. Klimm, C. Guguschev, D. J. Kok, M. Naumann, L. Ackermann, D. Rytz, M. Peltz, K. Dupré, M. D. Neumann, A. Kwasniewski, D. G. Schlom, and M. Bickermann, Crystal growth and characterization of the pyrochlore  $\text{Tb}_2\text{Ti}_2\text{O}_7$ , *CrystEngComm*, **19**, 3908 (2017).
- M. K. Reynolds and D. W. Paul, Determination of Diffusion Coefficients through a Polymer Membrane Using a Rotating Disc Electrode, *227th ECS Meet. Abstr.*, **MA2015-01**, 2224 (2015).
- M. von Stackelberg, M. Pilgram, and W. Toome, Bestimmung Von Diffusionskoeffizienten Einiger Ionen In Wassriger Lösung In Gegenwart Von Fremdelektrolyten 1, *Zeitschrift Für Elektrochem.*, **57**, 342 (1953).
- B. B. Bliznac, P. N. Ross, and N. M. Markovic, Oxygen electroreduction on  $\text{Ag}(111)$ : The pH effect, *Electrochimica Acta*, **52**, 2264 (1953).
- L. Jiang, A. Hsu, D. Chu, and R. Chen, Oxygen Reduction Reaction on Carbon Supported Pt and Pd in Alkaline Solutions, *J. Electrochem. Soc.*, **156**, B370 (2009).
- M. Stojimenović, M. Momčilović, N. Gavrilov, I. A. Pašti, S. Mentus, B. Jokić, and B. Babić, Incorporation of Pt, Ru and Pt-Ru nanoparticles into ordered mesoporous carbons for efficient oxygen reduction reaction in alkaline media, *Electrochimica Acta*, **153**, 130 (2015).
- L. An, M. Zhu, B. Dai, and F. Yu, Hollow palladium-copper bimetallic nanospheres with high oxygen reduction activity, *Electrochimica Acta*, **176**, 222 (2015).
- K. J. J. Mayrhofer, G. K. H. Wiberg, and M. Arenz, Impact of Glass Corrosion on the Electrocatalysis on Pt Electrodes in Alkaline Electrolyte, *J. Electrochem. Soc.*, **155**, P1 (2008).
- P. E. Kasatkin, E. Härk, R. Jäger, and E. Lust, Oxygen Reduction Reaction in Alkaline Solution: Influence of Catalyst Loading and Carbon Support Characteristics, *ECS Trans.*, **64**, 115 (2015).
- N. Alexeyeva, K. Tammeveski, A. Lopez-Cudero, J. Solla-Gullón, and J. M. Feliu, Electroreduction of oxygen on Pt nanoparticle/carbon nanotube nanocomposites in acid and alkaline solutions, *Electrochimica Acta*, **55**, 794 (2010).
- M. A. Subramanian, G. Aravamudan, and G. V. Subba Rao, Oxide pyrochlores — A review, *Prog. Solid State Chem.*, **15**, 55 (1983).
- Y. Lee, J. Suntivich, K. J. May, E. E. Perry, and Y. Shao-Horn, Synthesis and Activities of Rutile  $\text{IrO}_2$  and  $\text{RuO}_2$  Nanoparticles for Oxygen Evolution in Acid and Alkaline Solutions, *J. Phys. Chem. Lett.*, **3**, 399 (2012).